# Localization of neurons from extracellular footprints

Mélina Scopin, Giulia L.B. Spampinato, Olivier Marre, Samuel Garcia, Pierre Yger

Journal of Neuroscience Methods 412 (2024) 110297

Contents lists available at ScienceDirect

Journal of Neuroscience Methods

journal homepage: www.elsevier.com/locate/jneumeth

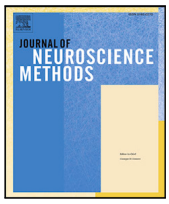

# Localization of neurons from extracellular footprints

Mélina Scopin [a,*], Giulia L.B. Spampinato [a], Olivier Marre [a], Samuel Garcia [c], Pierre Yger [a,b]

[a] Institut de la Vision, Sorbonne Université, INSERM, Paris, France
[b] Lille Neurosciences & Cognition (lilNCog) – U1172 (INSERM, Lille), Univ Lille, CHU Lille 59045 Lille, France
[c] Centre de Recherche en Neuroscience de Lyon, CNRS, Lyon, France

ARTICLE INFO

*Keywords:*
Spike sorting
Neurons
Ground-truth
Electrophysiology
Source localization

ABSTRACT

**Background:** High density microelectrode arrays (HD-MEAs) are now widely used for both *in-vitro* and *in-vivo* recordings, as they allow spikes from hundreds of neurons to be recorded simultaneously. Since extracellular recordings do not allow visualization of the recorded neurons, algorithms are needed to estimate their physical positions, especially to track their movements when the are drifting away from recording devices.
**New Method:** The objective of this study was to evaluate the performance of multiple algorithms for neuron localization solely from extracellular traces (MEA recordings), either artificial or obtained from mouse retina. The algorithms compared included center-of-mass, monopolar, and grid-based algorithms. The first method is a barycenter calculation. The second algorithm infers the position of the cell using triangulation with the assumption that the neuron behaves as a monopole. Finally, grid-based methods rely on comparing the recorded spike with a projection of spikes of hypothetical neurons with different positions.
**Results:** The Grid-Based algorithm yielded the most satisfactory outcomes. The center-of-mass exhibited a minimal computational cost, yet its average localization was suboptimal. Monopolar algorithms gave cell localizations with an average error of less than 10 μm, but they had considerable variability and a high computational cost. For the grid-based method, the variability was smaller, with satisfactory performance and low computational cost.
**Comparison with Existing Method(s):** The accuracy of the different localization methods benchmarked in this article had not been properly tested with ground-truth recordings before.
**Conclusion:** The objective of this article is to provide guidance to researchers on the selection of optimal methods for localizing neurons based on MEA recordings.

## 1. Introduction

Spike sorting is the algorithmic process of recovering the individual activity of neurons from extracellular recordings (see Einevoll et al., 2012 for reviews). With the tremendous increase in the density of electrodes and the advent of high density microelectrode arrays (HD-MEAs), one can hope to recover the activities of hundreds, if not thousands, of neurons with a single spike resolution. In consequence, the subject of spike sorting has become a topic of considerable interest (Lefebvre et al., 2016; Yger et al., 2018; Pachitariu et al., 2023; Buccino et al., 2022). However, it is important to emphasize that extracellular recordings are performed blindly: the identity and location of the cells within the vicinity of the electrodes are unknown.

The fact that the nature and position of cells are missing poses numerous problems in ensuring the validity and robustness of spike sorting pipelines. To understand why, it is worth noting that most, if not all, modern algorithms extract the isolated activities of neurons from extracellular recordings in a standardized manner. After an initial detection of peaks in the extracellular traces, the differentiation of the extracellular waveforms emitted by the individual neurons is usually performed by a clustering algorithm. For this purpose, the dimensionality of the waveforms (centered around the detected peaks) is reduced to a *so-called* "feature space". All dimensionality reduction techniques that have been used to perform this projection (Lefebvre et al., 2016) have in common that they project the waveforms into an abstract feature space, and their projections must be learned on a subset of the data before application. Once the extracellular waveforms have been found, all spikes are classically detected *via* a greedy template-matching procedure (Pachitariu et al., 2023; Yger et al., 2018; Lee et al., 2020), resolving the spatio-temporal overlaps or *so-called* "collisions" (Garcia et al., 2022).

* Corresponding author.
*E-mail address:* melina.scopin@inserm.fr (M. Scopin).

https://doi.org/10.1016/j.jneumeth.2024.110297
Received 31 May 2024; Received in revised form 23 September 2024; Accepted 29 September 2024
Available online 9 October 2024

Recently, however, the question of bypassing such a feature extraction step has been raised, especially in the context of *in-vivo* non-stationary recordings, to address the problems of drifting tissue (Steinmetz et al., 2021). Indeed, spike sorting is a blind-source separation problem, where one need to disambiguate the sources (the neurons) based on the extracellular traces. However, *in vivo*, cells are likely to slowly drift away from their initial positions because of the pressure release in the tissue after the insertion of the probe. The exact nature of these drifts is unpredictable: they can have arbitrary time constants, either be abrupt and discontinuous or slow and continuous. The only certainty is that drifts distort the spatiotemporal signatures of individual spikes, recorded extracellularly, and thus the "feature space" aforementioned.

To track these moving neurons, it would be important to have a proper estimation of their movement and position in order to disambiguate them efficiently. The possibility of quickly obtaining an estimate of the position of cells from the shapes of their extracellular waveforms would potentially facilitate spike sorting procedures and simplify the handling of physical drifts. Although the putative localization of neurons has often been rather naively estimated by several spike sorting algorithms using a simple center-of-mass (CoM) algorithm depending on their electrical signatures, more sophisticated algorithms, taking into account some biophysical properties of the cells, have been proposed to infer such positions (Hurwitz et al., 2022; Pachitariu et al., 2023; Buccino et al., 2018).

In this article, we will try to quantify the pros and cons of the latest techniques used by modern sorters, and the extent to which the positions of the cells can be reliably inferred from the extracellular traces. The accuracy of these localization techniques has not yet been properly tested with ground-truth recordings and therefore, it is difficult to know the extent to which such "estimated" positions could be used to correctly estimate true physical properties of the cells, such as drift. We will thus compare how accurate such localization methods could be, either with synthetic or with ground-truth recordings obtained from *in-vitro* recordings in the mouse retina.

## 2. Materials and methods

### 2.1. Notations

Throughout the article, vector variables are represented by the $\vec{}$ notation. We use $\vec{w}_i(t) \in \mathbb{R}^{N\times M}$ to represent the spatiotemporal waveforms emitted by the neuron $i$ at time $t$, where $N$ is the total number of channels and $M$ is the number of time samples (by default, we cut out the 2 ms signal at a sampling rate of 32 kHz, which makes $M = 64$). We will use the notation $\vec{w}_i^F(t)$ to refer to a one dimensional representation (of size $\mathbb{R}^{N\cdot M}$) of the waveforms where all channels are concatenated. We further use the term Ground-Truth (GT) to refer to fully controlled variables in our synthetic recordings.

### 2.2. Synthetic recordings

Using the `MEArec` Python package (Buccino and Einevoll, 2020), 250 multicompartment biophysical neuron models were created based on experimental data from layer 5 of the rat cortex. In summary, the intracellular activity of these neurons was simulated using `NEURON` (Hines and Carnevale, 1997) including trans-membrane currents. Neurons are located on top of a square high density microelectrode array (HD-MEA), arranged as a grid of 16 times 16 channels, each spaced by 30 µm. From the simulated extracellular currents, extracellular action potentials were simulated using the `LFPy` package (Lindén et al., 2014), and 10-minute recordings were generated at a sampling rate of 32 kHz. The firing rate of excitatory neurons was set at 5 Hz with a standard deviation of 1 Hz, and the firing rate of inhibitory neurons was set at 15 Hz with a standard deviation of 3 Hz. Both cell types had a refractory period of 2 ms. Neuronal firing was simulated in a Poisson process. The noise level was set at a value of 10 µV. The obtained recordings were processed with a Butterworth bandpass filter of order 3 between 300 and 6000 Hz, and each channel is divided by its own noise level, so that the variance on a given channel is approximately 1. To assess the possibilities offered by various localization methods with respect to the drift correction algorithm applied *in-vivo*, we also generated data in Fig. 5 using a Neuropixel-like layout of 128 channels (Steinmetz et al., 2021). 250 cells were added near the electrode, generated exactly as in the case described above.

### 2.3. Experimental recordings

The experiments were carried out according to institutional animal care standards. For the ground-truth recordings, electrophysiological recordings were obtained from *ex-vivo* isolated retinas of rd1 mice (4/5 weeks old). The retinal tissue was placed in AMES medium (Sigma-Aldrich, St Louis, MO; A1420) bubbled with 95% O2 and 5% CO2 at room temperature, on a MEA (252 10 µm electrodes spaced 30 µm apart; Multichannel Systems, Reutlingen, Germany) with the layer of ganglion cells facing the electrodes. Borosilicate glass electrodes (BF100-50, Sutter Instruments) were filled with AMES with a final impedance of 6–9 MΩ. Cells were imaged using a custom-built inverted DIC microscope (Olympus BX 71) equipped with a high-sensitivity CCD camera (Hamamatsu ORCA -03G) and recorded using an Axon Multiclamp 700B patch clamp amplifier set in current zero mode. In the data shown in Fig. 4A, 5 neurons were recorded on 4 intact retinas. Recording durations of 5 min were analyzed, and the datasets are already available online (Spampinato et al., 2018).

### 2.4. Localization of the cells

In order to estimate the putative positions of the somas, several types of methods are considered in this study.

#### 2.4.1. Center of mass algorithms

The first algorithm, most commonly used in the literature, is a straightforward estimate *via* a center-of-mass estimation. More precisely, assuming that a neuron $i$ has its waveform $\vec{w}_i(t)$ defined on several channels $a \in \{1, \dots, n_{\text{channels}}\}$, we can compute, for example, the peak-to-peak values $\text{ptp}^i(a)$ on each channel. Since each channel has a physical position $\vec{p}_a = (x_a, y_a)$ in 2D space, we can obtain, for each neuron $i$, its barycenter or its so-called center-of-mass $CoM(i)$, such as:

$$CoM(i) = \frac{\sum_a \text{ptp}^i(a)\vec{p}(a)}{\sum_a \text{ptp}^i(a)} \tag{1}$$

Note that the choice of the peak-to-peak feature is arbitrary, and one could use other features instead. For example, one could think of the $\|-\|_2$ norm over each channel or the values $\vec{w}_i(t_a)$ where $t_a$ is the time of the absolute minimum of the template. These two features are used as "energy" and "peak voltage" in the article.

#### 2.4.2. Monopolar approximations

The second method used in the article is called the monopole approximation. As in Varol et al. (2021a), the idea is to consider the cell as a monopole and to infer its position by triangulation given the template amplitudes recorded on all channels. More precisely, assuming that the cell behaves as a monopole, we can exploit the fact that each spike is detectable on several channels $a$ simultaneously: i.e., if the position of cell $i$ is $\vec{p}_i = (x_i, y_i, z_i)$, we have several observations of the form:

$$\text{ptp}^i(a) = \frac{k_i}{\sqrt{(x_a - x_i)^2 + (y_a - y_i)^2 + (z_a - z_i)^2}} \tag{2}$$

with the term $k_i$ including the magnitude of the current and propagation properties of the tissue (see Buccino et al., 2018). Therefore,

to obtain the position of the neuron, one can try to find $(x_i, y_i, z_i, k_i)$ in order to minimize the following cost function $\Phi(x, y, z, k)$.

$$\Phi(x, y, z, k) = \sum_a (\text{ptp}^i(a) - \frac{k}{\sqrt{(x_a - x_i)^2 + (y_a - y_i)^2 + (z_a - z_i)^2}})^2 \quad (3)$$

The position of the neuron estimated via a Monopolar approximation is thus

$$Mon(i) = \underset{x,y,z,k}{\text{argmin}}\, \Phi(x, y, z, k) \quad (4)$$

To minimize the cost function, the scipy.optimize toolbox (Virtanen et al., 2020) was used, with the BFGS (Broyden–Fletcher–Goldfarb–Shanno) algorithm. Again, the choice of peak-to-peak values as a feature could be questioned. In this work, similar to the case of the center-of-mass, we will also study the refined cases of "energy" or "peak voltage", for which different features are used to infer the source.

#### 2.4.3. Grid-based convolutions

The third localization method used in this article is called Grid convolution. This is a slight extension of the method developed in Pachitariu et al. (2023) and explained in Garcia et al. (2023), in order to also estimate a putative depth of the neurons. The idea behind this localization method is to create an exhaustive catalog of artificial templates $\vec{f}_{n\in1,\dots,k}(t)$ at known positions $\vec{p}_n = (x_n, y_n, z_n)$ and to estimate the position of a given spike $\vec{w}_i(t)$ projected on this basis. If the spatial resolution of this grid is finer than that of the recording channels, one might expect the resolution of the localization estimates to improve.

The scalar products $\beta_{i,n} = \vec{w}_i^F(t)\vec{f}_n^F(t)$ of the spike are computed with all templates on the basis, and then, keeping only those that are positive, the position $Grid(i)$ of the spike is estimated as a weighted sum of the positions, with weights equal to the scalar product between the spike and these templates.

$$Grid(i) = \frac{\sum_n \beta_{i,n}\vec{p}_n}{\sum_n \beta_{i,n}} \quad (5)$$

To create the fake templates, the typical waveform $H(t)$ of a spike on a single channel is estimated, and then duplicated on all nearby channels, with weight factor $g$ depending on the distance $d$ between the position of the artificial templates $\vec{p}_n$ and the channel locations $\vec{p}_a$. Therefore, writing $d_{a,n} = \|\vec{p}_n - \vec{p}_a\|$, we have the following.

$$\vec{f}_n(a, t) = H(t)g(d_{a,n}) \quad (6)$$

The exact nature of the weight factor $g$ is arbitrary. For example, in Kilosort (Pachitariu et al., 2023), the authors used a weight decay that follows a decaying exponential profile such that $g(d_{a,n}) = e^{-d_{a,n}^2/\sigma}$. A caveat here is that the distances are only calculated in the 2d space $(x, y)$, but the depth can be approximated by varying the spread of $sigma$. In the following, this solution will be referred to as the Grid method with the mode "gaussian_2d". One other option would be to consider a simple decaying exponential such as $g(d_{a,n}) = e^{-d_{a,n}/\kappa}$ (Segev et al., 2004), and compute the distances in the full 3d space. In the article this solution will be called Grid with the mode "exponential_3d", and in all the following, we fix $\kappa = 2.5\,\mu\text{m}$. By extending the grid into 3 dimensions, we can get a putative estimate of the depth of the neurons. The ones that are far apart will have a larger footprint on the MEA, compared to the ones close to the recording sites. To reduce the scattering of the scalar products when there are too many templates in the basis, we perform the estimation in Eq. (5) only on the top 5% of the positive scalar products. Details of both implementations can be found in Buccino et al. (2020).

#### 2.4.4. Control method

Finally, as a control measure, we also used the position of the channel where the minimum voltage is obtained, either for an averaged template, or for individual spikes. This method will be referred to as the "Peak Channel", and has the advantage of not requiring any computations.

### 2.5. Estimation of the positions on a single-spike basis

In the article, we estimated the variability of the positions when estimated on a single-spike basis. However, in a real-life situation, the spike sorting algorithms would not have access to the exact spike times, and the detection threshold will add an extra layer of noise as a slight jitter in the temporal or spatial domain. To take that into account, for each ground-truth spike time, we look in a small spatio-temporal neighborhood for the largest peak that might have been detected by any peak detection algorithm. The estimated positions are thus estimated on this slightly jittered time.

## 3. Results

In this work, we wanted to assess the extent to which we could extract the putative positions of neurons from their extracellular traces. To do this, we used MEArec (Buccino and Einevoll, 2020) to generate a 10-minute artificial recording with 250 randomly placed neurons (see Methods and Fig. 1A). The cell firing rate was fixed at 5 Hz for excitatory cells and 15 Hz for inhibitory cells, and the extracellular traces (for a subset of recording channels) can be seen in Fig. 1B. To characterize the activity of a given neuron $i$, spike sorting algorithms usually try to identify the *so-called* "templates" $\vec{w}_i(t)$, that is, spatiotemporal motifs elicited when the neuron $i$ fires an action potential on all its nearby recording channels. This is shown in Fig. 1C, for a selected neuron $i$ in the center of the HD-MEA. Only channels within a given radius $\rho$ of 100 μm around the position of the cell are shown, which carry all the information. As can be seen, the template $\vec{w}_i(t)$ is smooth, as it is an average of many spikes shown in Fig. 1D. We then looked at the precision of different localization methods, both at the averaged template level (see Fig. 1E) and at the single-spike level (which is more noisy and possibly corrupted by other spikes, see Fig. 1F). In fact, to infer the position of a given neuron, one might be tempted to work only at the template level. But, to track the potential drift or movement of a specific neuron over time, it may be necessary to infer its position based on a single spike. For all methods, the localization variance, when estimated on a single-spike basis, is high.

In the following, we compare three different approaches to infer the positions of the neurons from their extracellular traces (see Methods). To cover all cases found in the literature, we made some minor modifications to the center-of-mass and Monopolar methods to get a broader overview of the possibilities and to explore their performance as a function of the feature chosen. In fact, both methods can be based on different features (peak-to-peak, $\|-\|_2$ norm or the peak voltage, i.e., the time of the absolute extrema of the template; see Methods). For the Grid Convolution method, we assessed the accuracy of two estimators noted "gaussian_2d" and "exponential_3d". Finally, we compared these different methods to the "Peak Channel", which considers the electrode where the highest peak was recorded as the position of the neuron.

First, we looked at averaged template levels, which are more commonly used. We expect that smoothed averaged waveforms would lead to accurate and precise estimation of cell positions. As can be seen in Fig. 2A, all methods make smaller errors for larger templates (high signal-to-noise ratio). Similarly, as we can see in Fig. 2B, there is a tendency for all methods to make larger errors when the cells are far from the center of the HD-MEA. This is because for cells at the edges, the templates are partly outside of the field of view, and thus positions are incorrectly estimated. In addition, note that CoM-based methods, by definition, cannot recover a position outside the HD-MEAs. The Monopolar approximation and the Grid convolution methods both appear to outperform all CoM-based methods, with average errors of, respectively, $\approx$ 7 μm and $\approx$ 9 μm. Except for the CoM-based peak voltage estimator, all the methods presented here allow for a better localization of the neuron than approximating its position with the Peak Channel. These errors are summarized in Fig. 2C. It is important

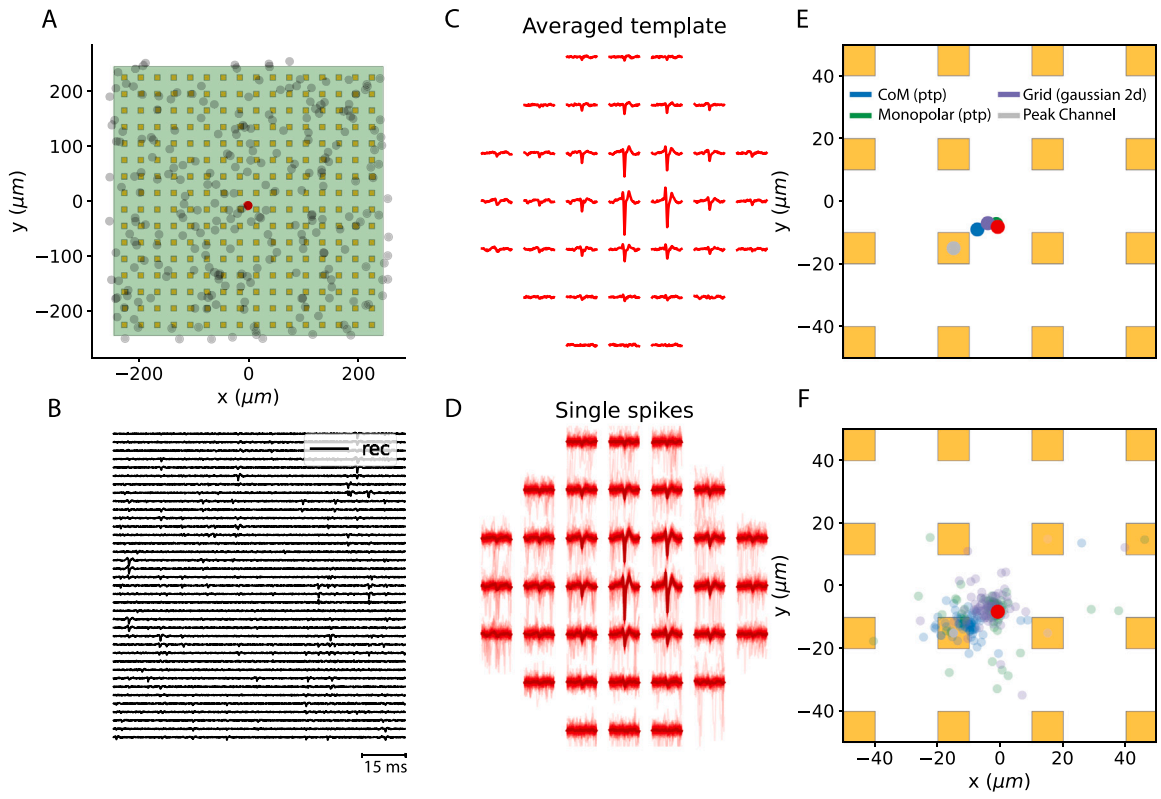


**Fig. 1.** Illustration of the generation of artificial recordings. **A** The layout of a 256-channel HD-MEA with 30 μm spacing between each electrode is displayed, and the black dots correspond to the positions of (some of) the artificial neurons. The red dot highlight the particular case of the neuron whose waveforms are shown in panels **C, D**. **B** 100 ms of extracellular recordings, shown only for a few channels. **C** The template of the neuron highlighted in red in panel A (averaged over many spikes). **D** 100 waveforms taken from single spikes of the same neuron (as in **C**), superimposed. **E** Localization, with several localization algorithms (see Methods), performed on the averaged template. Red dot illustrates the real position of the generated template. **F** Same as **E**, but when localizing individual spikes.

to stress that despite similarities in the overall curves in Fig. 2, the localization methods are not necessarily making the errors on the same neurons (data not shown).While some cells (with a small signal-to-noise ratio and/or located distant from the center) present challenges for all methods, the discrepancies across localization methods are relatively distributed for the other cells.

If we look at the precision of these measures but on individual spikes rather than on averaged templates, the overall picture is different. The same trends can be seen in Figs. 2D and E, where all methods show sensitivity to template amplitude and distance from the center of the HD-MEA. In Fig. 2F and G, we have plotted the average of the median absolute deviations (mads) of errors across all single-spike realizations. While we can see that the Monopolar approximation has a relatively small mean error, its mads are larger than some CoM-based methods, and more importantly, the variance of these mads is also large. From these observations (see Fig. 2H), we conclude that CoM-based methods yield significant error and substantial variability, while the Monopolar approximation is more accurate (on average) but has a large variance. The Peak Channel method demonstrates minimal variability but significant error. The Grid convolution methods show better results, with lower errors than pure CoM-based errors and lower variances compared to Monopolar-based methods.

In order to understand how some of these methods are affected by their parameters, we decided to investigate their robustness with respect to key parameters that could affect them. In Fig. 3 (first column), we looked at the influence of the time window around the peaks used to compute the methods. For CoM or Grid-Based methods (Fig. 3A, C), this time window has almost no effect on the averaged errors. For the Monopolar methods, (Fig. 3B), as expected, the larger the window, the larger the error, as we start to include more noise than the signal of interest. This method seems to have an optimal accuracy of around 0.5 ms, and degrades for lower and higher values. Similarly, in Fig. 3 (second column), we examined the influence of the radius $\rho$ around the main peak. The larger the radius, the more channels (or templates in the case of the Grid method) are used to estimate the positions. Selecting more channels means collecting noise, and thus degrading the quality of the estimation, except for the Grid-Based methods. The optimal radius for the other methods was found to be approximately 50 μm. In Fig. 3 (third column) and for a particular case ($\rho = 50\,\mu m$, $\tau = 1$ ms) we looked at errors as a function of the axes ($x$, $y$ and $z$). To measure how such an estimate can be used to predict depth, we calculated the correlation coefficient between the real coordinates ($x$, $y$, and $z$) and the estimated coordinates. As we can see from Fig. 3 the correlation coefficient in the $z$ -axis is much worse than in the 2D space, probably due to lack of information. In addition, the final column illustrates these values as functions of the averaged errors performed (expressed as a percentage), and we can appreciate that both the Monopolar and the Grid-based methods are able to accurately predict the values in the $z$-axis. Not only are the relative relationships kept, but also to some extent the values themselves.

As artificial recordings do not fully reflect the complexity of physiological recordings, we measured the accuracy of each algorithm using ground-truth recordings from *ex-vivo* retinas. Using intracellular recordings performed simultaneously with HD-MEA recordings, we obtained the real positions of 5 cells, as well as the timing of their spikes. This allowed us to calculate the averaged template for each cell and predict its localization with the different algorithms. Since we can localize the tip of the glass pipet (see Fig. 4A), we know approximately the position of the neuron (at least in the $(x, y)$ plane) and we also know the timing of its spikes, so we can obtain the perfect extracellular signature from the HD-MEA recordings (see Methods, see Fig. 4B). Applying our localization methods to extracellular templates and/or individual

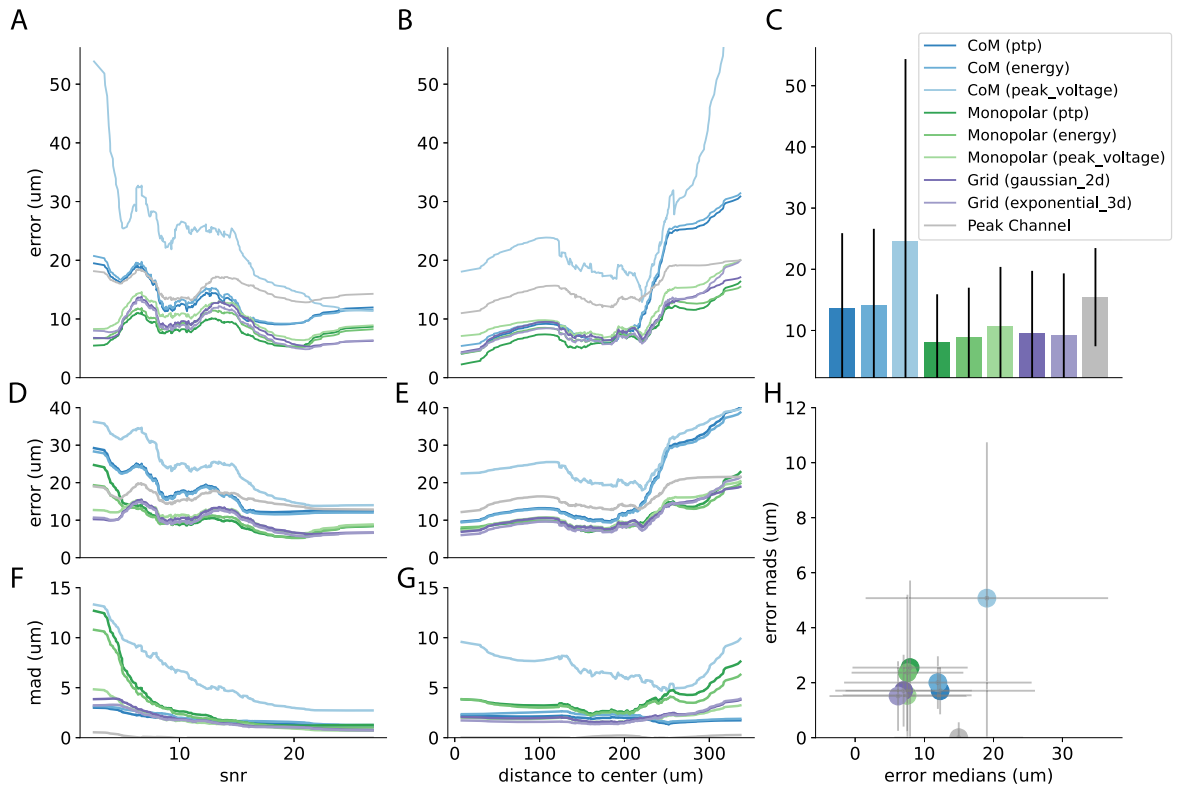


**Fig. 2.** Localization errors as a function of the methods. **A** Error in the estimated positions of the averaged templates as a function of the signal-to-noise ratio (snr), for several inference methods (see Methods) **B** Same as **A**, but ordered by the distance of the cells from the center of the array. **C** Mean error (over the 250 ground-truth templates) between the positions of the ground-truth templates and those estimated from the averaged templates. Error bars show the standard deviations on the templates. **D** Same as in **A**, but the error is calculated as the mean, over neurons, of the errors calculated on single-spike realizations as a function of the snr. **E** Same as in **D**, but the error is computed as the mean, over neurons, of the errors computed on single-spike realizations, as function of the distance to the center. **F** Median absolute deviation of the error, over neurons, for errors computed on single-spike realizations as function of the snr. **G** The same as in **F**, but as a function of the distance to the center. **H** Median errors and Median absolute Deviations over all neurons and their individual spikes. The gray bars represent the variability along the median error (i.e., the degree of accuracy of the mean errors) or along the median absolute deviations (i.e., the extent of variation in the errors).

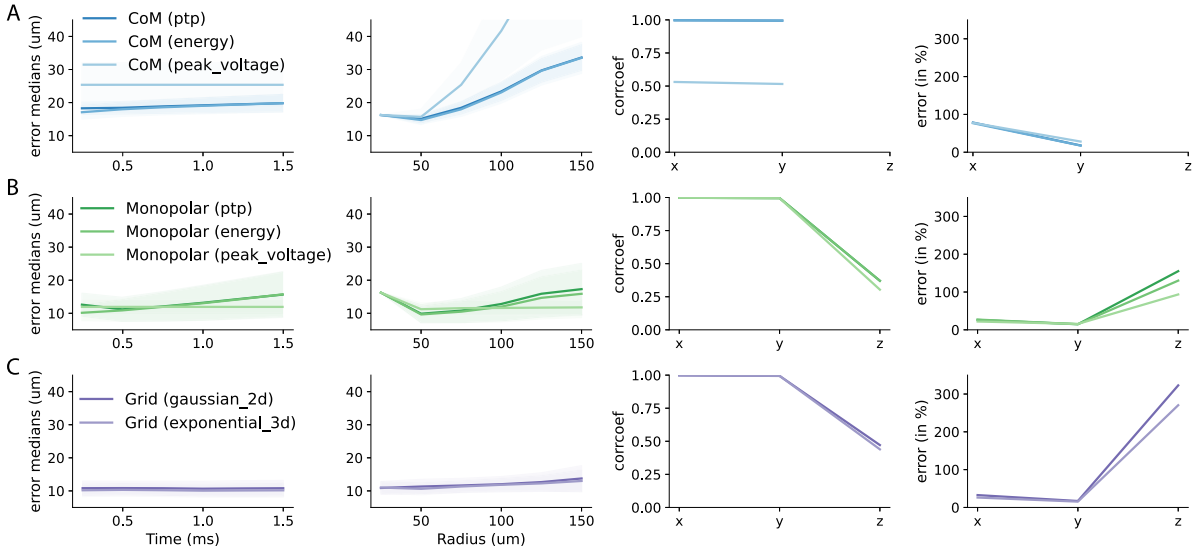


**Fig. 3.** Influence of the parameters on the localization methods. **A** Impact of the parameters for Center of Mass based methods. From left to right: 1. Median of all errors, over all templates, as a function of the time window around the spikes used to estimate the peak-to-peak feature. The shaded areas represent the median absolute deviations over all templates. 2. Same, but as a function of the local radius $\rho$, in microns, used to restrict the area around the peak (see Methods). 3. Correlation coefficients between the real x, y and z coordinates and the found ones. 4. Error (in %) realized in the x, y and z dimensions. **B** Same as **A** but for Monopolar based methods. **C** Same as **A** but for Grid-based methods.

spikes, we can obtain putative estimates of the positions (see Fig. 4C). We can see that the localization errors are very similar on average between neurons when performed at the template level (see Fig. 4D). For all cells, we can notice that Monopolar and grid-based methods tend to behave similarly, whereas the Peak Channel method strongly differs. An issue arises from the inability to effectively know the source from

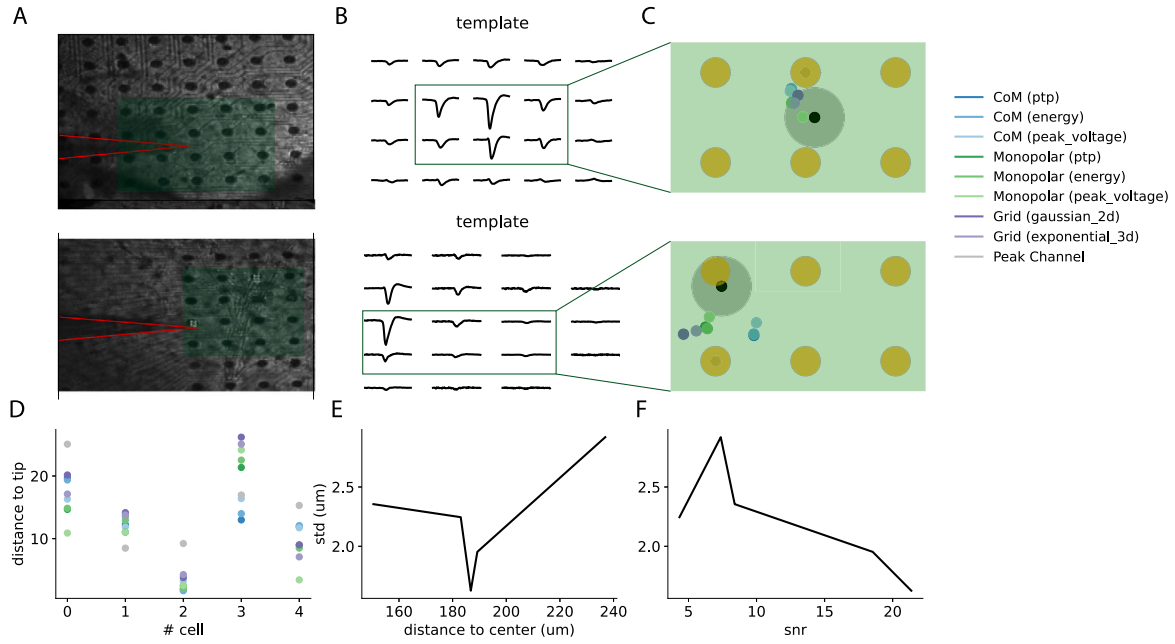


**Fig. 4.** Accuracy of cell localization with ground-truth recordings. **A** Illustration of the HD-MEA layout, with the tip of the juxtacellular electrode (in red) patching two ganglion cells (two rows). Green areas represent the closest channels shown in following panels. **B** The waveforms triggered by ground-truth neurons, averaged over their spikes (obtained from juxtacellular recordings) **C** The estimated position of these two particular neurons, obtained with different localization methods (see Methods), compared to the putative physical position in black (located with the tip of the electrode) **D** Distance to the tip obtained when estimating positions from the averaged templates, over 5 cells in 5 different retinas, for all localization methods. **E** Variances over all positions given by localization methods as a function of the distance to the center of the MEA for the tip of the electrode. **G** The same as in **F** but as a function of the signal-to-noise ratio of the patched ground-truth neuron.

which the action potential originates, specifically the initial segment of the axon, which is not visible in this dataset. As a consequence, the only discernible outcome is the relative agreement across the localization methods. As shown in Fig. 4E, the variance between all the positions found is low ($\approx 2.5\,\mu m$) and appears to vary as a function of the signal-to-noise ratio of the patched neuron (Fig. 4F). It should be noted that the Peak Channel and CoM-based methods often lead to slight outliers in localization (see Fig. 4D), it can thus be posited that Grid-based and Monopolar methods exhibit consistent behavior, without the necessity for further assumptions regarding the location of the actual source of the action potential.

While we have shown in this article that the Monopolar approximation appears to be slightly more accurate for inferring position from extracellular recordings, we have also shown that it comes at the cost of higher variability on a single-spike basis. This is inconvenient, since modern spike-sorting algorithms rely on the localization of individual spikes to perform drift tracking. In particular, all recent methods that try to perform a non-rigid registration of the activity profile of neurons (see Buccino et al., 2022 for a review) assume that one can correctly estimate the histogram, along one dimension, of the activity profile as a function of the localization methods. As illustrated in Fig. 5, we addressed this aspect using a Neuropixel-like probe layout (as detailed in the Methods section) with the objective of restricting ourselves to the 1D scenario, which represents the sole case currently addressed by the registration methods (Pachitariu et al., 2023; Boussard et al., 2021; Varol et al., 2021b). As can be seen in Fig. 5A, the distribution of cells along the depth can give rise to different distributions of estimated positions depending on the localization method (see Fig. 5B), using a $4\,\mu m$ bin for the width of the histogram.

To measure how different the estimated distributions are from the ground-truth, we compared, for various localization methods, a selection of metrics computed between the discrete histograms (obtained with various bin sizes) and the ground-truth histogram. In Fig. 5C, we can see that 1 minus the correlation coefficient between the estimated and the real histograms (varying the bin width, and along the $y$-axis) is consistently lower for the Monopolar methods. This means that the histograms of the positions estimated using Monopolar methods are more similar to those obtained from the ground-truth spikes, which should facilitate the work of the registration procedures. The same is true for the Bhattacharyya distance (data not shown), often used as a distance between 1D distributions. If we look at the effect of the bin sizes, i.e. the resolution at which we are looking at the histograms to perform the correlation, we can see in Fig. 5C that for all bin sizes (and either we are looking in the $y$ or $z$-axis), the same trend is visible: largest distances are obtained for CoM-based methods, the Grid is an in between, and the Monopolar approximation is the best, with a slight preference for the "energy" or "peak voltage" implementations. It should be noted that for very large spatial bins of histograms, the correlation is artificially increasing due to the fact that everything begins to appear essentially indistinguishable, resulting in similar-looking histograms.

However, estimating the activity profile of all spikes is costly and this is why some methods that rely on Monopolar approximations (Boussard et al., 2021; Varol et al., 2021a) are very time-consuming. As one can appreciate in Fig. 5D, the run time for Monopolar estimations is three times slower than the other methods, and this prevents, for large-scale and long recordings, a proper usage of such metrics. This is why the Grid-based methods seem to represent an optimal compromise in terms of performance and run times. This is confirmed in Fig. 5E showing 1 minus the correlation coefficient between the estimated and real histograms (varying the width of the bin) along the $z$-axis. As observed previously in Fig. 3, the Grid-based methods are also able, to some extent, to infer the relative relationships along the $z$-axis, thus offering some possibilities for downstream clustering algorithms and/or spike sorting pipelines.

## 4. Discussion

In this article, we reviewed the strengths and weaknesses of the three main methods used to estimate cell position from extracellular

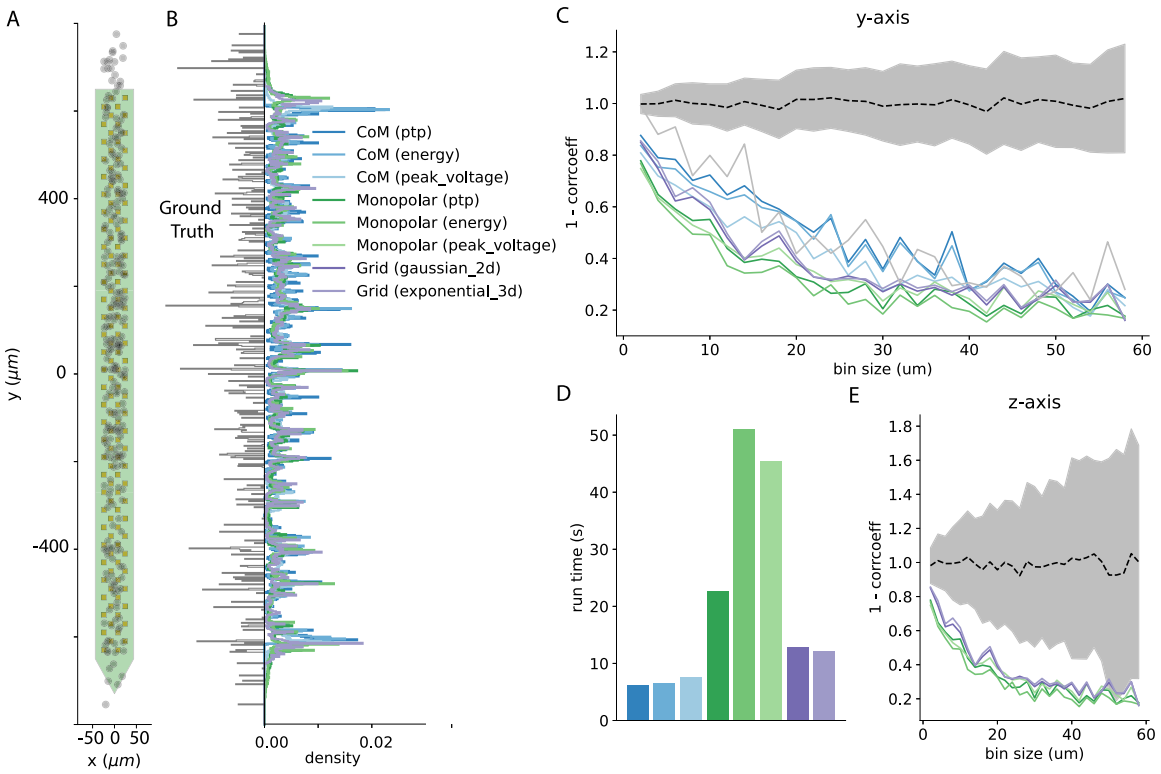


**Fig. 5.** Influence of the localization for drift correction algorithms. **A** A Neuropixel probe layout with cells generated uniformly in the vicinity of the electrodes. **B** Histogram of the distributions of the positions of all individual spikes, when using different localization schemes, and with a spatial bin of 4 μm. The ground-truth histogram (gt) is shown on the left as a reference. **C** 1 minus the correlation coefficient between the histograms obtained on the *y*-axis from the ground-truth positions and those estimated by several localization algorithms for different bin sizes. The dash dotted line represents a control level for uniformly drawn position along the *y*-axis, and the shaded gray area the variability of the measure. **D** Run times for the different localization methods. **E** Same as in **C**, but for several bin sizes used to compute the histograms in the *z*-axis.

traces in HD-MEA recordings. We compared the accuracy of the center-of-mass (CoM), Monopolar and Grid methods in localizing the precise positions of neurons in either artificial microelectrode array (high density MEA) recordings or real ground-truth recordings (n = 5). The CoM method relies on a simple barycenter calculation using either peak-to-peak (ptp), energy or peal voltage values as weights. When using ptp or energy, this method gave satisfactory results with a mean accuracy of $\approx$ 12 μm in the localization of the averaged templates of neurons. Using the peak-voltage metric seemed to greatly increase the error for artificial MEA recordings, but this was not the case for ground-truth recordings. We recommend using the CoM method for fast estimation of templates or single-unit positions. For more precise results, an alternative is to use the Monopolar method, which has been shown to achieve median localization errors of less than 10 μm for both templates and single units. However, this method demonstrated greater variability in the localization of single units and is also more computationally demanding, which raises questions about its suitability as an optimal tool for correcting drifts in recordings. The Grid method (as used in Kilosort 2, 2.5 and 3 Pachitariu et al., 2023) has a reasonable computational cost and offers relatively small errors in the localization of templates and single units (around 10 μm). This method provided better localization than the CoM method and less variability than the Monopolar method, standing as an in-between between the two inference schemes.

Both the Monopolar and the Grid Convolution methods allow for a 3-dimensional estimation of the unit positions. It can be observed that the error in the *z*-axis is significantly higher than the error in the $(x, y)$ axis. This was expected for the Monopolar method, as the estimation of the distance in the *z*-axis is highly dependent on the estimation of the spike amplitude and is highly under-constrained. Indeed, the waveform recorded from a nearby neuron with a small spike amplitude would be similar to that recorded from a neuron at a greater distance but with a larger spike amplitude. Nevertheless, the estimation of both the spike amplitude and the *z*-position could be useful, especially in the context of the increasing prevalence of 3D probes (Grob et al., 2020; Lycke et al., 2023; Wang et al., 2023; Suzuki et al., 2022).

Estimating the putative positions of neurons from extracellular footprints can be useful in several use cases. For example, in neuronal cultures and/or organoid *in-vitro*, it would be beneficial to estimate the location of cells, in order to evaluate the putative synaptic pathways between them. Alternatively, being able to estimate the positions of the neurons could be useful to correct for recording drifts *in-vivo*. As shown in Buccino et al. (2022), drifts are now a major bottleneck for chronic tracking of neurons over multiple days. So far, the best drift correction algorithms are based on ideas borrowed from computer vision (with non-rigid registration of the activity profiles Pachitariu et al., 2023; Boussard et al., 2021), and thus on putative positions of the neurons. Our findings demonstrate that, in order to estimate such activity profiles, grid-based methods are more reliable, with a satisfactory run time, and thus should be preferred over CoM or Monopolar alternatives.

However, it should be noted that the position estimated by all three methods is that of the axon initial segment (AIS), where the action potential is emitted. The relative position of the AIS to the soma can vary between different cell types and can even change with structural plasticity (Kuba, 2012). In the case of cultured neurons, the position of the AIS may show even more variability. Therefore, the position of the soma cannot be accurately determined from the position of the AIS, and despite some imaging studies suggesting that Monopolar methods are more accurate (Ghazal et al., 2023), more ground-truth experiments are needed to assess the extent by which cell bodies can be localized.

## CRediT authorship contribution statement

**Mélina Scopin:** Writing – review & editing, Writing – original draft, Visualization, Software, Project administration, Methodology,

Investigation, Formal analysis, Conceptualization. **Giulia L.B. Spampinato:** Writing – review & editing, Visualization, Validation, Software, Resources, Methodology, Investigation, Formal analysis, Data curation. **Olivier Marre:** Writing – review & editing, Visualization, Validation, Resources, Methodology, Investigation, Funding acquisition, Formal analysis, Data curation, Conceptualization. **Samuel Garcia:** Writing – review & editing, Visualization, Validation, Software, Formal analysis. **Pierre Yger:** Writing – review & editing, Writing – original draft, Visualization, Validation, Supervision, Software, Resources, Project administration, Methodology, Investigation, Funding acquisition, Formal analysis, Data curation, Conceptualization.

## Declaration of competing interest

The authors declare no competing interests.

## Data availability

All the code used in this work are part of the open source python project `spikeinterface` (Buccino et al., 2020), which can be found online. The ground-truth experiments used in this study are also available online (Yger et al., 2018).

## References


Boussard, J., Varol, E., Lee, H.D., Dethe, N., Paninski, L., 2021. Three-dimensional spike localization and improved motion correction for neuropixels recordings.

Buccino, A.P., Einevoll, G.T., 2020. Mearec: a fast and customizable testbench simulator for ground-truth extracellular spiking activity. Neuroinformatics 1–20.

Buccino, A.P., Garcia, S., Yger, P., 2022. Spike sorting: new trends and challenges of the era of high-density probes. Prog. Biomed. Eng. 4 (2), 022005.

Buccino, A.P., Hurwitz, C.L., Garcia, S., Magland, J., Siegle, J.H., Hurwitz, R., Hennig, M.H., 2020. SpikeInterface, a unified framework for spike sorting. Elife 9, e61834.

Buccino, A.P., Kordovan, M., Ness, T.r.V., Merkt, B., Häfliger, P.D., Fyhn, M., Cauwenberghs, G., Rotter, S., Einevoll, G.T., 2018. Combining biophysical modeling and deep learning for multielectrode array neuron localization and classification. J. Neurophysiol. 120 (3), 1212–1232.

Einevoll, G.T., Franke, F., Hagen, E., et al., 2012. Towards reliable spike-train recordings from thousands of neurons with multielectrodes. Curr. Opin. Neurobiol. 22 (1), 11–17.

Garcia, S., Buccino, A.P., Yger, P., 2022. How do spike collisions affect spike sorting performance? eNeuro 9 (5), ENEURO.0105–22.2022.

Garcia, S., Windolf, C., Boussard, J., Dichter, B., Buccino, A.P., Yger, P., 2023. A modular approach to handle in-vivo drift correction for high-density extracellular recordings.

Ghazal, M., Scholaert, C., Dumortier, C., Lefebvre, C., Barois, N., Janel, S., Tarhan, M.C., Colin, M., Buée, L., Halliez, S., Pecqueur, S., Coffinier, Y., Alibart, F., Yger, P., 2023. Precision of neuronal localization in 2D cell cultures by using high-performance electropolymerized microelectrode arrays correlated with optical imaging. Biomed. Phys. Eng. Express 9 (3).

Grob, L., Yamamoto, H., Zips, S., Rinklin, P., Hirano-Iwata, A., Wolfrum, B., 2020. Printed 3D electrode arrays with micrometer-scale lateral resolution for extracellular recording of action potentials. Adv. Mater. Technol. 5 (3), 1900517, _eprint: https://onlinelibrary.wiley.com/doi/pdf/10.1002/admt.201900517.

Hines, M.L., Carnevale, N.T., 1997. The NEURON simulation environment. Neural Comput. 9 (6), 1179–1209.

Hurwitz, C.L., Xu, K., Srivastava, A., Buccino, A.P., Hennig, M.H., 2022. Scalable spike source localization in extracellular recordings using amortized variational inference.

Kuba, H., 2012. Structural tuning and plasticity of the axon initial segment in auditory neurons. J. Physiol. 590 (22), 5571–5579.

Lee, J., Mitelut, C., Shokri, H., Kinsella, I., Dethe, N., Wu, S., Li, K., Reyes, E.B., Turcu, D., Batty, E., et al., 2020. YASS: Yet another spike sorter applied to large-scale multi-electrode array recordings in primate retina.

Lefebvre, B., Yger, P., Marre, O., 2016. Recent progress in multi-electrode spike sorting methods. J. Physiol. Paris 110 (4), 327–335.

Lindén, H., Hagen, E., Ł ęski, S., Norheim, E.S., Pettersen, K.H., Einevoll, G.T., 2014. LFPy: a tool for biophysical simulation of extracellular potentials generated by detailed model neurons. Front. Neuroinform. 7, 41.

Lycke, R., Kim, R., Zolotavin, P., Montes, J., Sun, Y., Koszeghy, A., Altun, E., Noble, B., Yin, R., He, F., Totah, N., Xie, C., Luan, L., 2023. Low-threshold, high-resolution, chronically stable intracortical microstimulation by ultraflexible electrodes. Pages: 2023.02.20.529295 Section: New Results.

Pachitariu, M., Sridhar, S., Stringer, C., 2023. Solving the spike sorting problem with Kilosort. Pages: 2023.01.07.523036 Section: New Results.

Segev, R., Goodhouse, J., Puchalla, J., Berry, M.J., 2004. Recording spikes from a large fraction of the ganglion cells in a retinal patch. Nat. Neurosci. 7 (10), 1154–1161.

Spampinato, G.L., Esposito, E., Yger, P., Duebel, J., Picaud, S., Marre, O., 2018. Ground truth recordings for validation of spike sorting algorithms.

Steinmetz, N.A., Aydin, C., Lebedeva, A., Okun, M., Pachitariu, M., Bauza, M., Beau, M., Bhagat, J., Böhm, C., Broux, M., et al., 2021. Neuropixels 2.0: A miniaturized high-density probe for stable, long-term brain recordings. Science 372 (6539).

Suzuki, I., Matsuda, N., Han, X., Noji, S., Shibata, M., Nagafuku, N., Ishibashi, Y., 2022. Large-area electrical imaging having single neuron resolution using 236,880 electrodes CMOS-MEA technology. Pages: 2022.11.09.515884 Section: New Results.

Varol, E., Boussard, J., Dethe, N., Winter, O., Urai, A., International, T., Churchland, A., Steinmetz, N., Paninski, L., 2021a. Decentralized motion inference and registration of neuropixel data. ISBN: 9781728176055, pp. 1085–1089.

Varol, E., Boussard, J., Dethe, N., Winter, O., Urai, A., Laboratory, T.I.B., Churchland, A., Steinmetz, N., Paninski, L., 2021b. Decentralized motion inference and registration of neuropixel data. In: ICASSP 2021-2021 IEEE International Conference on Acoustics, Speech and Signal Processing. ICASSP, IEEE, pp. 1085–1089.

Virtanen, P., Gommers, R., Oliphant, T.E., Haberland, M., Reddy, T., Cournapeau, D., Burovski, E., Peterson, P., Weckesser, W., Bright, J., van der Walt, S.J., Brett, M., Wilson, J., Millman, K.J., Mayorov, N., Nelson, A.R.J., Jones, E., Kern, R., Larson, E., Carey, C.J., Polat, İ., Feng, Y., Moore, E.W., VanderPlas, J., Laxalde, D., Perktold, J., Cimrman, R., Henriksen, I., Quintero, E.A., Harris, C.R., Archibald, A.M., Ribeiro, A.H., Pedregosa, F., van Mulbregt, P., SciPy 1.0 Contributors, 2020. SciPy 1.0: Fundamental algorithms for scientific computing in python. Nature Methods 17, 261–272.

Wang, P., Wu, E.G., Uluşan, H., Phillips, A.J., Hays, M.R., Kling, A., Zhao, E.T., Madugula, S., Vilkhu, R.S., Vasireddy, P.K., Hierlemann, A., Hong, G., Chichilnisky, E.J., Melosh, N.A., 2023. Direct-print three-dimensional electrodes for large-scale, high-density, and customizable neural interfaces. Pages: 2023.05.30.542925 Section: New Results.

Yger, P., Spampinato, G.L., Esposito, E., Lefebvre, B., Deny, S., Gardella, C., Stimberg, M., Jetter, F., Zeck, G., Picaud, S., et al., 2018. A spike sorting toolbox for up to thousands of electrodes validated with ground truth recordings in vitro and in vivo. Elife 7, e34518.